ACS OMEGA

http://pubs.acs.org/journal/acsodf

Article

Accelerated Oxidative Degradation of Phosphonium-Type Ionic Liquid with L-Prolinate Anion: Degradation Mechanism and CO_2 Separation Performance

Hiroi Sei, Yu Nagai Kanasaki, Kouki Oka, Norimitsu Tohnai, Yuki Kohno,* and Takashi Makino*

Cite This: *ACS Omega* 2023, 8, 21154−21161

Read Online

ACCESS | Metrics & More | Article Recommendations | Supporting Information

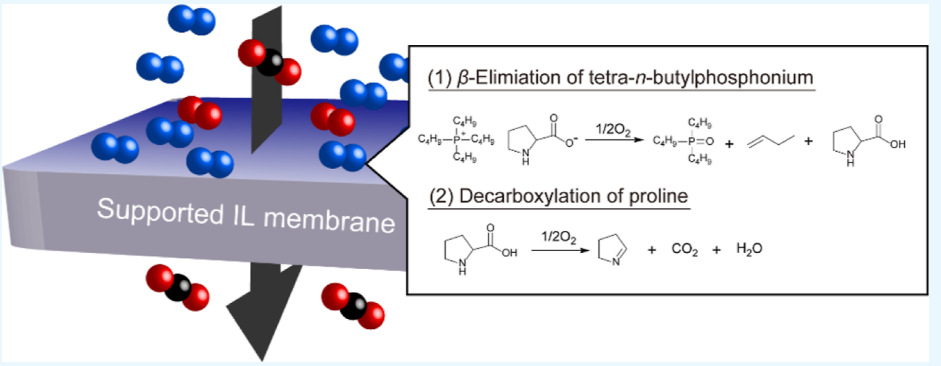

ABSTRACT: Amino acid ionic liquids (AAILs) are regarded as green alternatives to existing CO_2-sorptive materials because amino acids are readily available from renewable sources in large quantities. For widespread applications of AAILs, including direct air capture, the relationship between the stability of AAILs, especially toward O_2, and the CO_2 separation performance is of particular importance. In the present study, the accelerated oxidative degradation of tetra-*n*-butylphosphonium L-prolinate ([P_{4444}][Pro]), a model AAIL that has been widely investigated as a CO_2-chemsorptive IL, is performed using a flow-type reactor system. Upon heating at 120−150 °C and O_2 gas bubbling to [P_{4444}][Pro], both the cationic and anionic parts undergo oxidative degradation. The kinetic evaluation of the oxidative degradation of [P_{4444}][Pro] is performed by tracing the decrease in the [Pro]$^-$ concentration. Supported IL membranes composed of degraded [P_{4444}][Pro] are fabricated, and the membranes retain CO_2 permeability and CO_2/N_2 selectivity values in spite of the partial degradation of [P_{4444}][Pro].

INTRODUCTION

The large-scale deployment of negative emission technologies (NETs), which result in the net removal of greenhouse gases from the atmosphere, is required to mitigate global warming.[1,2] Among the various NETs reported to date, "Direct Air Capture" (DAC), which is a technology that can capture CO_2 from ambient air, experiences significant challenges owing to the very low concentration of CO_2 in the atmosphere (approximately 400 ppm). The concept of DAC was first reported by Lackner as one of the strategies for sequestering almost all produced CO_2 via decoupling point sources, such as power plants.[3] Toward the establishment of energy-efficient DAC systems, a number of CO_2-sorptive materials have been investigated and well described in the literature.[4,5] Ionic liquids (ILs) are regarded as a promising class of materials for CO_2 capture because ILs have favorable properties, including negligibly low vapor pressure, high thermal/chemical stability, and low flammability.[6,7] Moreover, the structural design of the component ions of ILs allows for the precise control of their affinities toward CO_2.[8−11] CO_2-chemisorptive ILs, including CO_2 reactive groups such as amino groups on anions and/or cations, have widely been investigated for CO_2 capture applications.[12] Among the amino-functionalized ILs, Ohno et al. first reported a series of amino acid ILs (AAILs) with 20 natural amino acids as anions, which were prepared by neutralization between various onium hydroxides and amino acids.[13−16] In the context of green and sustainable chemistry, AAILs offer greener alternatives to existing CO_2-chemsorptive materials because amino acids are readily available from renewable sources in large quantities. The solubility and reaction mechanism of CO_2 in the resulting AAILs have been widely investigated by several research groups.[17−23] In particular, AAILs with phosphonium cations and L-prolinate

Received: March 30, 2023
Accepted: May 10, 2023
Published: May 31, 2023

anion ($[Pro]^-$) show superior properties for CO_2 capture. Brennecke et al. reported that a trihexyl(tetradecyl)-phosphonium ($[P_{666,14}]^+$)-type AAIL with $[Pro]^-$ as the anion can absorb CO_2 in a 1:1 stoichiometry of CO_2/AAIL by stabilizing the carbamic acid moiety rather than through carbamate formation.[19,20] Matsuyama et al. investigated various facilitated transport membranes using tetra-*n*-butyl-phosphonium ($[P_{4444}]^+$)-based AAILs, and $[P_{4444}][Pro]$ exhibited CO_2 permeability and CO_2/N_2 selectivity considerably greater than the Robeson upper bounds under low CO_2 feed pressure conditions.[21,22]

For the widespread application of AAILs for CO_2 capture, the analysis of the relationship between thermal/chemical stability and CO_2 separation performance is particularly important. To date, very little research has been performed on the degradation of CO_2-chemsorptive ILs. The approaches for analyzing IL degradation can be grouped into methods associated with assessing mass changes, assessing chemical changes, and measuring changes in their properties. The simplest way to quantify the extent of degradation of ILs involves the mass loss of ILs by thermogravimetric analysis.[24−29] Brennecke et al. recently conducted isothermal mass loss measurements under N_2 and air environments from 373.15−473.15 K for several tetraalkylphosphonium ILs, including an AAIL with $[Pro]^-$ anion.[30] In the case of $[P_{666,14}][Pro]$, the temperature dependence of the mass loss rate constant follows the behavior described by Arrhenius' Law, showing activation energy (E_a) values of 49.4 kJ mol^{-1} in the N_2 atmosphere and 62.3 kJ mol^{-1} under air atmosphere. However, the relationship between changes in the chemical structures of AAILs and their CO_2 separation performance has not been determined. More specifically, the chemical stability of AAILs toward O_2 is one of the major factors to be considered in DAC applications owing to the relatively high O_2 concentration in air (i.e., 20.95%).

Herein, we report the oxidative degradation mechanism and kinetics of $[P_{4444}][Pro]$ as a model AAIL by establishing accelerated degradation procedures. In combination with various spectroscopic analyses, we propose degradation pathways for both $[P_{4444}]^+$ and $[Pro]^-$, in which the produced volatile compounds are released in the gaseous phase, while less volatile compounds remain in the AAIL phase. The kinetic evaluation of the oxidative degradation of $[P_{4444}][Pro]$ is conducted, and the membrane CO_2 separation performance for the degraded AAIL was evaluated by fabricating supported IL membranes.

EXPERIMENTAL SECTION

Synthesis of $[P_{4444}][Pro]$. $[P_{4444}][Pro]$ was prepared according to a previously reported procedure.[14] An equal molar amount of $[P_{4444}]OH$ (aqueous solution) and L-proline was mixed by stirring for at least 2 h until L-proline was completely dissolved. Water was removed using a rotary evaporator, and the residual viscous liquid was poured into a methanol/acetonitrile mixed solution (1:1 by volume) with dried molecular sieves (4 Å). The resulting solution was stored in a refrigerator overnight to precipitate unreacted L-proline. The solution was then filtered, followed by solvent removal and drying in vacuo at 50 °C to obtain $[P_{4444}][Pro]$. We prepared the AAIL several times, and neat-state ^1H-, ^{13}C-, and ^{31}P NMR spectroscopies of the prepared AAIL were performed to confirm their purities. The molar ratio of $[P_{4444}]^+/[Pro]^-$ was confirmed as 1:1, and no apparent peaks other than the component ions were observed in the ^1H NMR spectra (Figure S1). However, we determined a few small peaks other than that for $[P_{4444}][Pro]$ in both ^{13}C- and ^{31}P NMR spectra (Figures S2 and S3). The ^{13}C signals at δ = 28.4, 27.7, 24.3, and 13.6 ppm were assigned as tributylphosphine oxide. The ^{31}P signal also showed the presence of tributylphosphine oxide (δ = 60.9),[31] and another unknown peak was present at δ = 37.3. We checked the NMR spectra of the purchased $[P_{4444}]OH$ and determined that a few bottles of the reagent contained tributylphosphine oxide and an unknown impurity. To minimize any possible effects of such impurities, quantitative ^{13}C NMR spectroscopy for the prepared $[P_{4444}][Pro]$ was conducted, and $[P_{4444}][Pro]$ with peak intensities for tributylphosphine oxide no more than 3% of that for $[P_{4444}]^+$ was used in this study (Figures S1−S3, sample **1**).

Accelerated Degradation Experiments. In the present study, accelerated degradation experiments were conducted by heating and/or increasing the O_2 partial pressure. A schematic illustration of examining the accelerated degradation of $[P_{4444}][Pro]$ is shown in Figure S4. Three glass tubes, used for (i) gas pre-heating, (ii) sample loading for degradation, and (iii) trapping condensable gases at 25 °C, were placed in aluminum heating blocks (EYELA, PPS-5511), the temperature of which could be controlled individually. The AAILs were loaded into glass tubes (ii) in a glovebox, and the tubes were sealed with a rubber septum. The glass tubes were connected with stainless-steel needles and fluororesin tubes. The temperature of the loaded AAILs was monitored by directly inserting a fluororesin-coated thermocouple into the tubes. The AAILs were heated to the desired temperature with stirring (200 rpm). Subsequently, an individual or mixed (O_2 partial pressure of 20 kPa) O_2/N_2 gas was bubbled in the liquid phase to initiate the degradation. In the mixed gas, the O_2 partial pressure was 20 kPa. The flow rates of the individual and mixed O_2/N_2 gases were set at 100 and 20/80 cm^3/min, respectively, and were controlled with mass flow controllers (KOFLOC Corp., model 3660, Japan). To determine the degraded compounds in the gaseous phase, the outlet gas was continuously analyzed by mass spectrometry (MicrotracBEL, BELMASS II, Japan). Meanwhile, a small fraction of the AAILs were drawn up in a syringe at the desired time and characterized by NMR, acid−base titration, and CO_2/N_2 permeability measurements. For quantitative ^1H NMR measurements of the degraded AAIL samples, a D_2O solution containing DSS-d_6 was used as a solvent with an internal standard. The T_1 value was measured for protons on the δ carbon of $[Pro]^-$ (3.39 s), which was used to measure the concentration of $[Pro]^-$ in degraded $[P_{4444}][Pro]$. The delay time for the ^1H NMR measurement was set at 20 s, longer than $5T_1$. The temperature for the measurement was set to 40 °C.

Acid−Base Titration Measurements. The acid−base titration measurements were conducted by applying a previously reported method with modifications.[32] The degraded AAILs were diluted with deionized/degases water in a volumetric flask to a concentration of 10 mmol L^{-1}. The sample preparation was conducted in a water bath at 20.0 °C. The titration equipment consisted of a glass vessel with a thermostatic jacket (Metrohm, 6.1418.220, Switzerland), a magnetic stirrer, a pH glass electrode (DKK-TOA Corp., GST-5731C, Japan), and an automated pH meter unit (DKK-TOA Corp., MM-60R, Japan). The temperature of the titration cell was controlled at 20.0 °C with a chiller, and the solution

https://doi.org/10.1021/acsomega.3c02116
ACS Omega 2023, 8, 21154−21161

Scheme 1. Plausible Oxidative Degradation Pathway for Tetra-*n*-Butylphosphonium L-prolinate through (1) *β*-Elimination of Tetra-*n*-Butylphosphonium and Proton-Transfer to L-prolinate Anion and (2) Decarboxylation of Proline

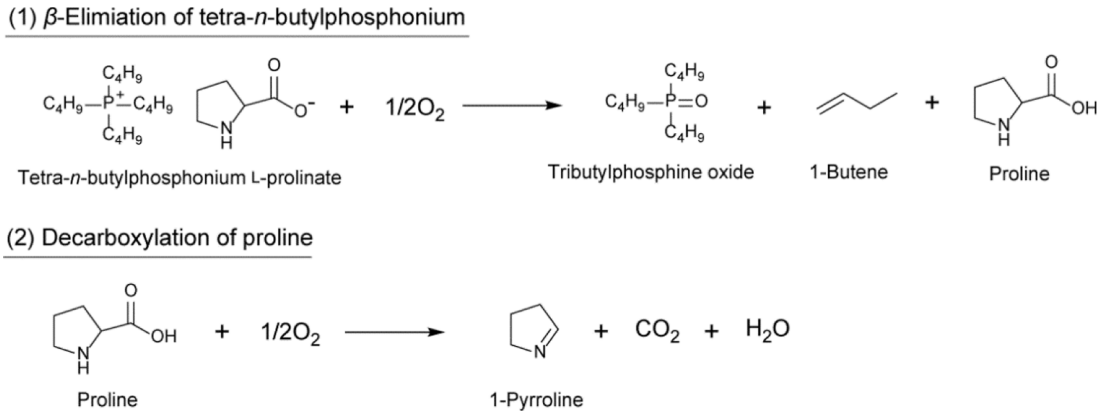

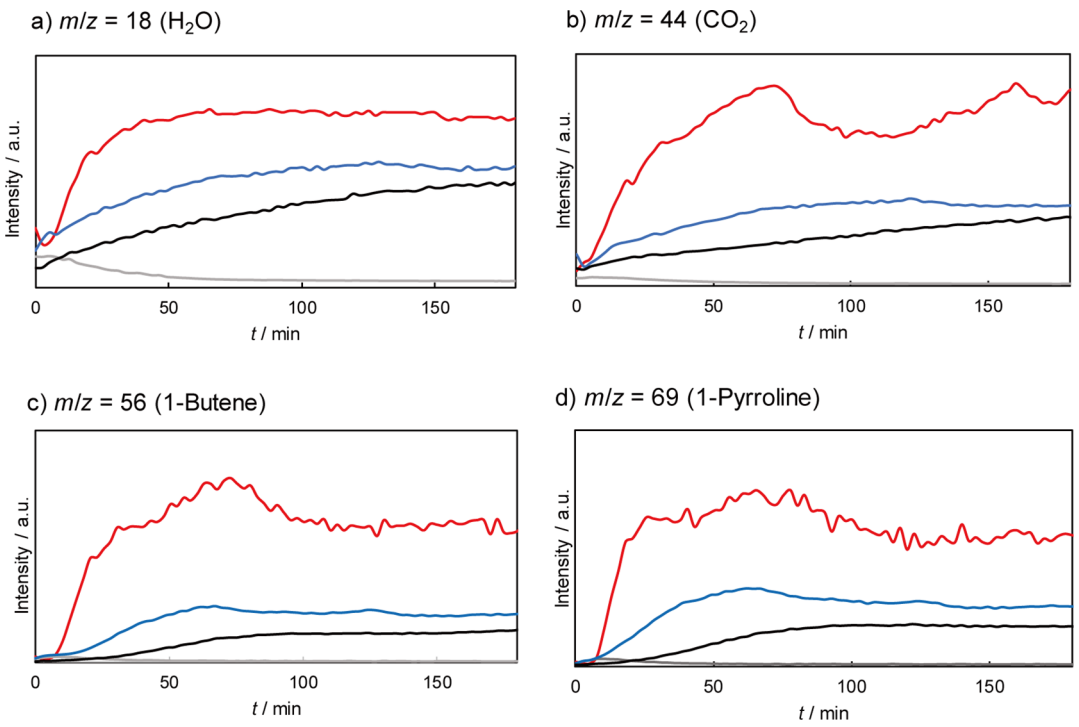

Figure 1. Time course of the online gas-phase mass peak intensities of (a) m/z = 18 (H_2O), (b) m/z = 44 (CO_2), (c) m/z = 56 (1-butene), and (d) m/z = 69 (1-pyrroline) under O_2 flow at 120 (black), 135 (blue), and 150 °C (red) and under N_2 flow at 150 °C (gray).

temperature was monitored by directly inserting a Pt thermocouple in the solution. 20 mL of the prepared AAIL solution were titrated with aqueous HCl (10 mmol L^{-1}). The HCl solution (0.2 mL) was added to the AAIL solution at a speed of 10 mL/min, and the resulting solution was stirred for 120 s. After storing the solution for another 120 s, the pH value was measured. The pH electrode was calibrated using three standard buffer solutions of with pH values of 4.01, 6.86, and 9.18.

Measurement of the CO_2/N_2 Gas Permeability for Supported Ionic Liquid Membranes. A schematic illustration of the CO_2/N_2 mixed gas permeation measurement is shown in Figure S5. Supported IL membranes using non-degraded and degraded [P_{4444}][Pro] were fabricated according to our previous report.[33] The filling rate of each IL in the membrane support (PTFE filter) was calculated to be 98∼99%, which is determined as a volume of IL loaded in a void of the PTFE filter. The membrane thickness was 30 μm, and the value was unchanged before and after loading the ILs. The membranes were placed in a stainless-steel cell and set in a thermostatic oven (ISUZU, DSN-113, Japan) at 40 °C. The feed and sweep gas flow rates were maintained at 400 and 100 cm^3/min, respectively. The flow rates of CO_2 and N_2 in the feed gas were controlled using mass flow controllers (HORIBA STEC Inc., SEC-E40, Japan). The feed- and sweep-side pressures were maintained at approximately atmospheric pressure. The flow rates were measured using a film flow meter (HORIBA STEC Inc., SF-1U, Japan). The gas composition of the permeated CO_2 and N_2 was determined by gas chromatography (GC, GC-8A, Shimadzu Co., Japan), wherein a Shincarbon ST column was used for the measurement (Shinwa Chemical Industries Ltd., Japan). Each gas analysis was repeated at least three times until the difference

https://doi.org/10.1021/acsomega.3c02116
ACS Omega 2023, 8, 21154−21161

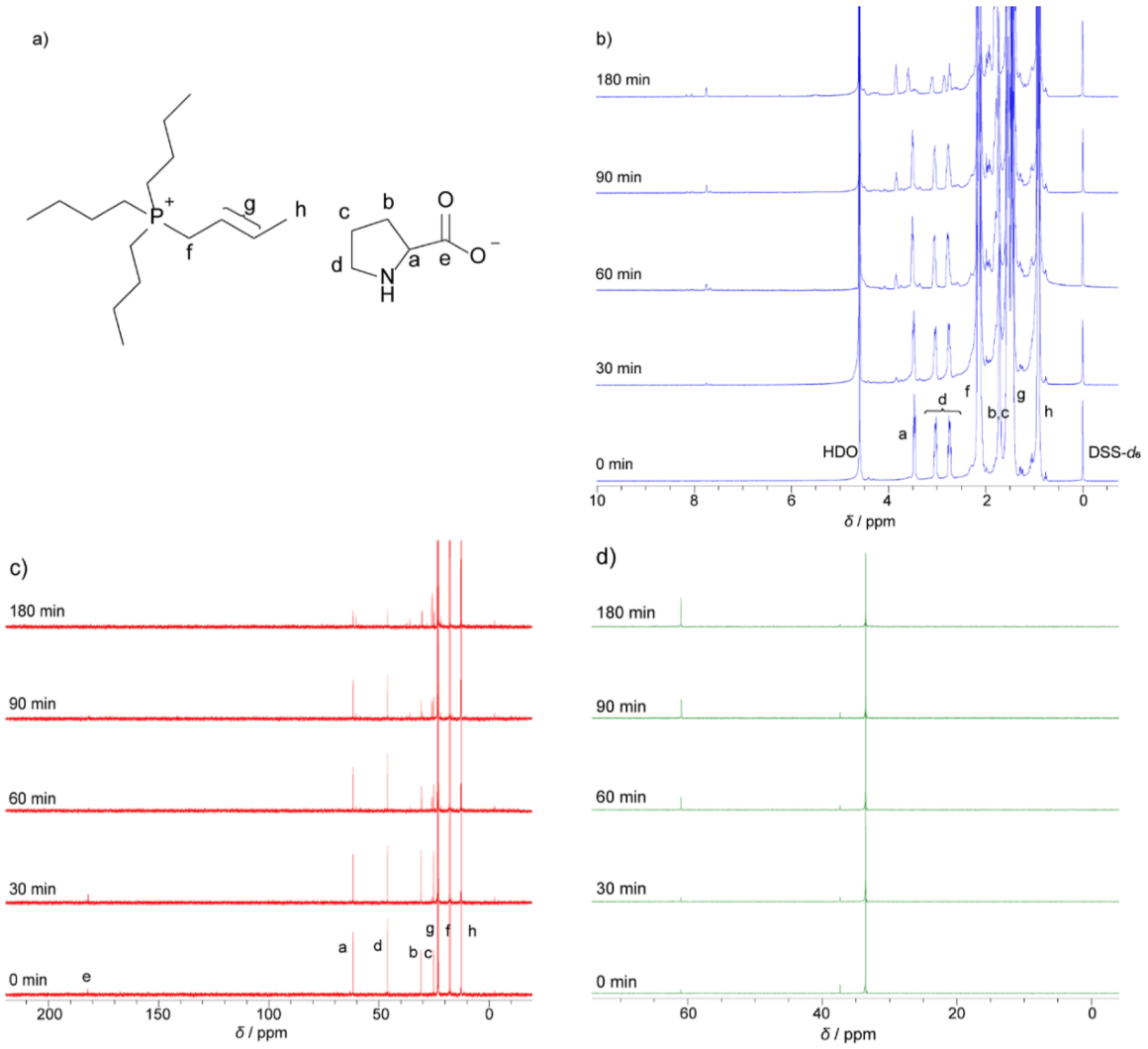

Figure 2. (a) Structure of tetra-*n*-butylphosphonium L-prolinate ($[P_{4444}][Pro]$) with NMR peak assignments. (b) ^{1}H-, (c) ^{13}C-, and (d) ^{31}P NMR spectra of $[P_{4444}][Pro]$ in D_2O after specific time intervals of O_2 degradation at 150 °C. 3-(Trimethylsilyl)-1-propane-1,1,2,2,3,3-d_6-sulfonic acid sodium salt (DSS-d_6) was used as an internal standard.

between the sequential CO_2 and N_2 peak areas as measured by GC was less than 1%.

RESULTS AND DISCUSSION

Distinct oxidative degradation pathways exist for $[P_{4444}]^+$ and $[Pro]^-$. Potential degradation reactions of alkylphosphonium cations include a nucleophilic substitution reaction at the α-carbon center, β-elimination, and phosphorous substitution.[34] Trialkyphosphines, trialkylphosphine oxides, alkanes, and alkenes are the resulting degradation products. In the case of β-elimination, the β-proton on the phosphonium cation is abstracted by a base in concert with the elimination of the alkene.[34] In the presence of O_2, substitution at the phosphorus can proceed to generate trialkylphosphine oxide. To promote β-elimination, a base (proton acceptor) is required. One plausible proton acceptor in $[P_{4444}][Pro]$ is a Lewis basic $[Pro]^-$ that can undergo protonation to form proline.[35] The oxidative degradation of proline was previously investigated in the presence of periodate, and decarboxylation was proposed as a mechanism for proline degradation.[36] As a consequence, some degradation compounds, including 1-pyrroline, CO_2, and H_2O, were produced.[36] Upon considering previous reports, it is assumed that the oxidative degradation pathway of $[P_{4444}][Pro]$ follows (**1**) the β-elimination of $[P_{4444}]^+$ concomitantly with the proton transfer to $[Pro]^-$, followed by (**2**) the decarboxylation of the generated proline, as shown in Scheme 1.

To prove the abovementioned hypothesis for the oxidative degradation of $[P_{4444}][Pro]$, preliminary studies were conducted to optimize accelerated degradation experiments for $[P_{4444}][Pro]$. Our initial trial utilized a batch-type stainless steel reactor equipped with a gas inlet/outlet and a pressure gauge. $[P_{4444}][Pro]$ was loaded in the reactor, and O_2 was bubbled in the AAIL at ambient temperature and pressure. Then, the degradation reaction was conducted above 120 °C in a closed system. After the reaction, we found that a pressure decrease occurred inside the reactor, indicating that the O_2 gas was consumed for the degradation reaction. To supply sufficient O_2 as a reactant for $[P_{4444}][Pro]$, as well as to analyze both the liquid and gaseous phases, we decided to construct a flow-type reactor system, as shown in Figure S4, in which an individual (101 kPa) or mixed (O_2 partial pressure of 20 kPa) O_2/N_2 gas was directly bubbled in $[P_{4444}][Pro]$ and an

https://doi.org/10.1021/acsomega.3c02116
ACS Omega 2023, 8, 21154−21161

outlet gas was continuously analyzed by online mass spectrometry.

Figure 1 shows the time course analysis of the mass intensities in the gaseous phase during the accelerated oxidative degradation of $[P_{4444}][Pro]$ at 120, 135, and 150 °C with O_2 gas bubbling (101 kPa). In the presence of O_2, the mass intensities for H_2O (m/z = 18), CO_2 (m/z = 44), 1-butene (m/z = 56), and 1-pyrroline (m/z = 69) increased, which increased further with increasing temperature. In contrast, there was no increase in the mass intensities under the N_2 atmosphere. This result clearly suggests that the oxidative degradation of $[P_{4444}][Pro]$ proceeds in the presence of O_2, and the degraded volatile compounds are in the gaseous phase, as proposed in Scheme 1. As shown in Figure 1c,d, the intensities of 1-butene and 1-pyrroline increased almost simultaneously, suggesting that degradation reaction (**2**) occurred immediately after degradation reaction (**1**) in Scheme 1. It should be noted here that a small portion of liquid was seen in a glass tube (iii) and/or a fluororesin tube between glass tubes (ii) and (iii) after the reaction (Figure S4), which indicates that some condensable gases emerged during the reaction. We did not conduct further analyses of these liquids in this study.

Subsequently, ^{1}H-, ^{13}C-, and ^{31}P NMR spectroscopic analyses were conducted for residual $[P_{4444}][Pro]$ after the oxidative degradation reaction at specific time intervals (Figure 2). As the reaction proceeded, the ^{1}H signals of $[Pro]^-$ gradually decreased (Figure 2b, δ = 3.45, 3.03, 2.74, and 1.71 ppm). Meanwhile, new peaks were detected in the ^{1}H NMR spectra (δ = 7.75, 3.84, and 2.72 ppm), which can be assigned to 1-pyrroline.[37] 1-Pyrroline has recently been identified as a semen-like odor emitted by chestnut flowers.[38] Degraded $[P_{4444}][Pro]$ emitted a similar odor. In the ^{13}C NMR spectra, the carboxylate carbon of $[Pro]^-$ was also diminished (Figure 2c, δ = 182 ppm). Furthermore, a signal for tributylphosphine oxide was detected in the ^{31}P NMR spectra, and its intensity increased upon progressing the reaction (Figure 2d, δ = 60.9).[31] Both mass spectrometry and NMR spectroscopy analyses clearly support the abovementioned mechanism in Scheme 1 that $[Pro]^-$ decarboxylation occurs during oxidative degradation, while $[P_{4444}]^+$ undergoes β-elimination.

Because the intensity of the ^{1}H signals for CO_2-chemsorptive $[Pro]^-$ decreased upon oxidative degradation, the $[Pro]^-$ concentration in the residual AAIL was used as an indicator for the oxidative degradation of $[P_{4444}][Pro]$. Accelerated oxidative degradation was conducted under an O_2 partial pressure of 101 kPa at 120, 135, and 150 °C using the same method as in Figure S4. The concentration of $[Pro]^-$ in the residual AAIL was determined using the quantitative ^{1}H NMR method, where 3-(Trimethylsilyl)-1-propane-1,1,2,2,3,3-d_6-sulfonic acid sodium salt (DSS-d_6) in D_2O was used as an internal standard. In addition, oxidative degradation at the same temperatures under an O_2 partial pressure of 20 kPa, assuming the concentration of O_2 in air, was also performed. The logarithm of concentration of $[Pro]^-$ in the residual AAIL ($\ln C_A$) was determined and plotted as a function of degradation time (Figures S6 and S7). The decrease in $[Pro]^-$ concentration under an O_2 partial pressure of 20 kPa proceeded rather slowly so that the degradation reactions under both conditions were carried out for 24 h. As shown in Figures S6 and S7, a linear decrease in the logarithm of the $[Pro]^-$ concentration was observed at each temperature and O_2 partial pressure condition. These plots were used to analyze the kinetics of the degradation of $[P_{4444}][Pro]$.

In the present study, the kinetics for oxidative degradation of $[P_{4444}][Pro]$ should be described as follows

$$r = k[C_A]^a[C_{O_2(g)}]^b \quad (1)$$

where r, k, C_A, and $C_{O_2(g)}$, respectively, denote oxidative degradation rate, rate constant, concentration of $[Pro]^-$, and concentration of O_2 in the gaseous phase. Both exponents a and b denote partial orders of reaction. In this study, the O_2 pressure and gas flow rate were set to 20/101 kPa and 100 cm^3/min, respectively, which were assumed to be sufficient to maintain the O_2 concentration constant. In addition, side reactions were assumed to occur negligibly. With these assumptions, we used a pseudo-first-order rate expression for the analysis.

The pseudo-first-order rate expression at a constant temperature is represented as follows

$$-\frac{dC_A}{dt} = k'C_A \quad (2)$$

where k' is the pseudo-first-order rate constant. The rate expressions in eq 2 can be converted to the integrated form, as shown in eq 3

$$C_A = C_{A0}e^{-k't} \quad (3)$$

where C_{A0} denotes the initial concentration of $[Pro]^-$, and t is time. The k' value was determined at different temperatures from the slope of the linear fitting of ln C_A–t plots shown in Figures S6 and S7. The temperature dependence of the pseudo-first-order rate constant is expressed by the Arrhenius equation as follows

$$\ln k' = \ln A - \frac{E_a}{RT} \quad (4)$$

where E_a is the molar activation energy and A is the pre-exponential factor.

Figure 3 illustrates the Arrhenius plot for the oxidative degradation of $[P_{4444}][Pro]$. It was found that the temperature

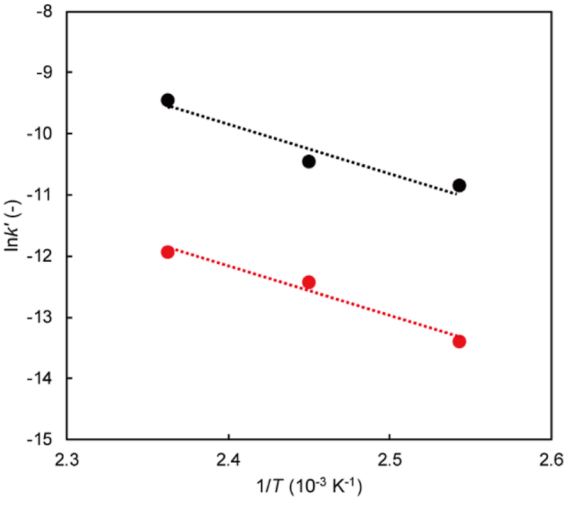

Figure 3. Arrhenius plot for degradation rates of tetra-*n*-butylphosphonium L-prolinate ($[P_{4444}][Pro]$) versus the inverse of temperature under O_2 pressures of 101 (black) and 20 kPa (red).

https://doi.org/10.1021/acsomega.3c02116
ACS Omega 2023, 8, 21154−21161

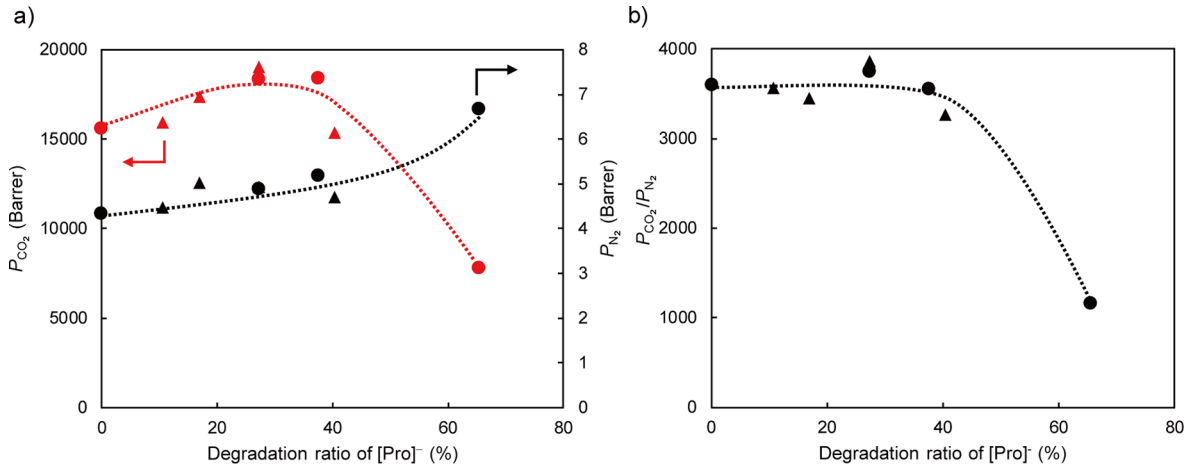

Figure 4. Effect of the degradation ratio of $[Pro]^-$ on the CO_2 separation performance for supported ionic liquid membranes. (a) CO_2 permeability (P_{CO_2}) and N_2 permeability (P_{N_2}). (b) CO_2/N_2 permeability selectivity (S_{CO_2/N_2}). The degraded samples were obtained through oxidative degradation at an O_2 pressure of 101 kPa at 135 (triangles) and at 150 °C (circles).

dependence of the pseudo-first-order rate constant followed the Arrhenius equation, and similar activation energy (E_a) values were observed at different O_2 partial pressures. The E_a values under O_2 partial pressures of 101 and 20 kPa were calculated as 62.0 ± 9.8 and 67.9 ± 4.4 kJ/mol, respectively, which are analogous to the reported values of $[P_{666,14}][Pro]$ that were determined by isothermal thermogravimetric analysis in air.[30]

To analyze the relationship between the extent of the degradation and CO_2 separation performance, the degraded $[P_{4444}][Pro]$ was impregnated in a porous Teflon film to prepare supported IL membranes (SILMs), and the gas permeability from a mixed feed gas containing CO_2/N_2 (CO_2 partial pressure: 40 Pa) was evaluated. The degraded samples were obtained after being heat treated at 135 or 150 °C under an O_2 atmosphere (101 kPa). The CO_2 permeability (P_{CO_2}), N_2 permeability (P_{N_2}), and CO_2/N_2 permeability selectivity ($S_{CO_2/N_2} = P_{CO_2}/P_{N_2}$) for the prepared SILMs were plotted as a function of the degradation ratio (%), which was calculated using the following equation

$$\text{degradation ratio (\%)} = \frac{C_{A0} - C_A}{C_{A0}} \times 100 \quad (5)$$

where C_{A0} and C_A denote the initial concentrations of $[Pro]^-$ and $[Pro]^-$ concentrations, respectively, after the oxidative degradation.

As shown in Figure 4a, the degradation ratio was not linearly correlated with P_{CO_2}. Compared to the non-degraded sample, higher P_{CO_2} values were observed upon increasing the degradation ratio, and a further increase in the specific degradation ratio steeply lowered the P_{CO_2} value. On the other hand, P_{N_2} values gradually increased with increasing degradation ratios. Accordingly, the S_{CO_2/N_2} values maintained the degradation ratio up to approximately 40% and significantly decreased above this ratio (Figure 4b). This tendency was analogously seen in the degraded AAILs obtained by oxidative degradation at 135 and 150 °C.

In general, the separation of CO_2 through facilitated transport membranes proceeds as follows. The reactive carriers in the membranes react with CO_2 to produce CO_2-carrier complexes, which are transported across the membranes. The back reaction occurred on the permeate side, releasing CO_2 and regenerating the carriers. Meanwhile, the transport of N_2 proceeds via a solution-diffusion mechanism, where N_2 is physically absorbed in the membranes, followed by diffusion through the membranes and desorption at the permeate side. Various properties influence the CO_2 permeability, such as CO_2 solubility, CO_2 absorption and desorption rate, viscosity, and the enthalpy of the solution of CO_2. Because the concentration of the CO_2 carrier (i.e., $[Pro]^-$) decreases upon degradation, the CO_2 solubility in the membranes may decrease, which reduces the moles of CO_2 permeated through the membranes. An acid−base titration for degraded $[P_{4444}][Pro]$ showed that base concentration values decreased upon proceeding with oxidative degradation (Figure S8). However, high values of P_{CO_2} and S_{CO_2/N_2} were maintained despite the decrease in $[Pro]^-$. One plausible factor that retains the high CO_2 permeation could be the reduced viscosity of the degraded $[P_{4444}][Pro]$. Because of the high boiling point of tributylphosphine oxide, a certain amount of tributylphosphine oxide may remain in $[P_{4444}][Pro]$, even after treating the SILMs under reduced pressure conditions. Such low-molecular-weight and neutral compounds, which do not possess strong interaction abilities, such as electrostatic interactions and/or hydrogen bonding, tend to lower the viscosity of ILs. Eventually, the diffusion of CO_2-carrier complexes may be improved throughout the membranes. Furthermore, the diffusion of N_2 increases by lowering the viscosity. In addition, the solubility of N_2 increases in the presence of neutral compounds, owing to the increase in free volume and decrease in density.[39] This affects the increase in P_{N_2} values upon $[P_{4444}][Pro]$ degradation. Further analyses on the relationship between the physico-chemical properties of the degraded $[P_{4444}][Pro]$, as well as other AAILs, and the CO_2 separation performance, will be conducted.

CONCLUSIONS

In summary, the accelerated oxidative degradation of $[P_{4444}][Pro]$ resulted in the β-elimination of $[P_{4444}]^+$ and decarboxylation of $[Pro]^-$ (Scheme 1). The generated compounds, including H_2O, CO_2, 1-butene, and 1-pyrroline, were present in the gaseous phase, while 1-pyrroline was also

https://doi.org/10.1021/acsomega.3c02116
ACS Omega 2023, 8, 21154−21161

present in the residual liquid phase. The less volatile tributylphosphine oxide remained in the liquid phase. The kinetics for the oxidative degradation of $[Pro]^-$ in the temperature range from 120 to 150 °C followed a pseudo-first-order reaction equation. During the degradation of $[P_{4444}][Pro]$, the P_{CO_2} and S_{CO_2/N_2} values remained within a specific range of degradation ratios. Our ongoing investigations include developing the current accelerated degradation method that acquires information on the long-term stability and/or degradation mechanism in a short period of time to evaluate the feasibility of various CO_2-chemsorptive ILs prior to large-scale demonstrations.

■ ASSOCIATED CONTENT

Supporting Information

The Supporting Information is available free of charge at https://pubs.acs.org/doi/10.1021/acsomega.3c02116.

Experimental details and characterization of $[P_{4444}][Pro]$ after oxidative degradation (PDF)

■ AUTHOR INFORMATION

Corresponding Authors

Yuki Kohno − *National Institute of Advanced Industrial Science and Technology (AIST), Sendai 983-8551, Japan;* orcid.org/0000-0003-3913-3444; Email: yuki-kouno@aist.go.jp

Takashi Makino − *National Institute of Advanced Industrial Science and Technology (AIST), Sendai 983-8551, Japan;* orcid.org/0000-0002-3618-154X; Email: makino.t@aist.go.jp

Authors

Hiroi Sei − *National Institute of Advanced Industrial Science and Technology (AIST), Sendai 983-8551, Japan; Department of Applied Chemistry and Center for Future Innovation (CFi), Graduate School of Engineering, Osaka University, Osaka 565-0871, Japan;* orcid.org/0009-0008-5273-9460

Yu Nagai Kanasaki − *National Institute of Advanced Industrial Science and Technology (AIST), Sendai 983-8551, Japan;* orcid.org/0000-0002-3057-5388

Kouki Oka − *Department of Applied Chemistry and Center for Future Innovation (CFi), Graduate School of Engineering, Osaka University, Osaka 565-0871, Japan;* orcid.org/0000-0001-6806-2767

Norimitsu Tohnai − *Department of Applied Chemistry and Center for Future Innovation (CFi), Graduate School of Engineering, Osaka University, Osaka 565-0871, Japan;* orcid.org/0000-0001-7051-7599

Complete contact information is available at: https://pubs.acs.org/10.1021/acsomega.3c02116

Author Contributions

H.S. performed the oxidative degradation reaction of $[P_{4444}][Pro]$ by establishing and optimizing accelerated degradation methods. Y.N.K. fabricated supported IL membranes and analyzed their CO_2/N_2 permeability. H.S. and Y.N.K. contributed equally to the manuscript. K.O., N.T., Y.K., and T.M. designed the study and oversaw the experimental work. The manuscript was written with contributions from all authors. All authors have approved the final version of the manuscript.

Notes

The authors declare no competing financial interest.

■ ACKNOWLEDGMENTS

This study was partially supported by the Grants-in-Aid for Scientific Research (20H02548 and 22K14732) from MEXT, Japan. K.O. also acknowledges support from the LNest Grant from Nipponham, the FUSO Innovative Technology Fund, the Masuya-kinen Basic Research Foundation, and the Shorai Foundation for Science and Technology.

■ REFERENCES

(1) Smith, P.; Davis, S. J.; Creutzig, F.; Fuss, S.; Minx, J.; Gabrielle, B.; Kato, E.; Jackson, R. B.; Cowie, A.; Kriegler, E.; et al. Biophysical and Economic Limits to Negative CO_2 Emissions. *Nat. Clim. Change* **2016**, *6*, 42−50.

(2) Minx, J. C.; Lamb, W. F.; Callaghan, M. W.; Fuss, S.; Hilaire, J.; Creutzig, F.; Amann, T.; Beringer, T.; de Oliveira Garcia, W.; Hartmann, J.; et al. Negative Emissions—Part 1: Research Landscape and Synthesis. *Environ. Res. Lett.* **2018**, *13*, 063001.

(3) Lackner, K. S. A. Guide to CO_2 Sequestration. *Science* **2003**, *300*, 1677−1678.

(4) Shi, X.; Xiao, H.; Azarabadi, H.; Song, J.; Wu, X.; Chen, X.; Lackner, K. S. Sorbents for the Direct Capture of CO_2 from Ambient Air. *Angew. Chem., Int. Ed.* **2020**, *59*, 6984−7006.

(5) Sanz-Pérez, E. S.; Murdock, C. R.; Didas, S. A.; Jones, C. W. Direct Capture of CO_2 from Ambient Air. *Chem. Rev.* **2016**, *116*, 11840−11876.

(6) Wasserscheid, P.; Welton, T. *Ionic Liquids in Synthesis*; Wiley-VCH: Weinheim, Germany, 2008.

(7) Armand, M.; Endres, F.; MacFarlane, D. R.; Ohno, H.; Scrosati, B. Ionic-Liquid Materials for the Electrochemical Challenges of the Future. *Nat. Mater.* **2009**, *8*, 621−629.

(8) Ramdin, M.; de Loos, T. W.; Vlugt, T. J. H. State-of-the-Art of CO_2 Capture with Ionic Liquids. *Ind. Eng. Chem. Res.* **2012**, *51*, 8149−8177.

(9) Cui, G.; Wang, J.; Zhang, S. Active Chemisorption Sites in Functionalized Ionic Liquids for Carbon Capture. *Chem. Soc. Rev.* **2016**, *45*, 4307−4339.

(10) Zeng, S.; Zhang, X.; Bai, L.; Zhang, X.; Wang, H.; Wang, J.; Bao, D.; Li, M.; Liu, X.; Zhang, S. Ionic-Liquid-Based CO_2 Capture Systems: Structure, Interaction and Process. *Chem. Rev.* **2017**, *117*, 9625−9673.

(11) Forse, A. C.; Milner, P. J. New Chemistry for Enhanced Carbon Capture: Beyond Ammonium Carbamates. *Chem. Sci.* **2021**, *12*, 508−516.

(12) Bates, E. D.; Mayton, R. D.; Ntai, I.; Davis, J. H. CO_2 Capture by a Task-Specific Ionic Liquid. *J. Am. Chem. Soc.* **2002**, *124*, 926−927.

(13) Fukumoto, K.; Yoshizawa, M.; Ohno, H. Room Temperature Ionic Liquids from 20 Natural Amino Acids. *J. Am. Chem. Soc.* **2005**, *127*, 2398−2399.

(14) Kagimoto, J.; Fukumoto, K.; Ohno, H. Effect of Tetrabutylphosphonium Cation on the Physico-Chemical Properties of Amino-Acid Ionic Liquids. *Chem. Commun.* **2006**, 2254−2256.

(15) Fukumoto, K.; Kohno, Y.; Ohno, H. Chiral Stability of Phosphonium-Type Amino Acid Ionic Liquids. *Chem. Lett.* **2006**, *35*, 1252−1253.

(16) Ohno, H.; Fukumoto, K. Amino Acid Ionic Liquids. *Acc. Chem. Res.* **2007**, *40*, 1122−1129.

(17) Zhang, J.; Zhang, S.; Dong, K.; Zhang, Y.; Shen, Y.; Lv, X. Supported Absorption of CO_2 by Tetrabutylphosphonium Amino Acid Ionic Liquids. *Chem.—Eur. J.* **2006**, *12*, 4021−4026.

(18) Zhang, Y.; Zhang, S.; Lu, X.; Zhou, Q.; Fan, W.; Zhang, X. Dual Amino-Functionalised Phosphonium Ionic Liquids for CO_2 Capture. *Chem.—Eur. J.* **2009**, *15*, 3003−3011.

(19) Gurkan, B. E.; de la Fuente, J. C.; Mindrup, E. M.; Ficke, L. E.; Goodrich, B. F.; Price, E. A.; Schneider, W. F.; Brennecke, J. F.

Equimolar CO_2 Absorption by Anion-Functionalized Ionic Liquids. *J. Am. Chem. Soc.* **2010**, *132*, 2116−2117.
(20) Brennecke, J. F.; Gurkan, B. E. Ionic Liquids for CO_2 Capture and Emission Reduction. *J. Phys. Chem. Lett.* **2010**, *1*, 3459−3464.
(21) Kasahara, S.; Kamio, E.; Ishigami, T.; Matsuyama, H. Effect of Water in Ionic Liquids on CO_2 Permeability in Amino Acid Ionic Liquid-Based Facilitated Transport Membranes. *J. Membr. Sci.* **2012**, *415−416*, 168−175.
(22) Moghadam, F.; Kamio, E.; Matsuyama, H. High CO_2 Separation Performance of Amino Acid Ionic Liquid-Based Double Network Ion Gel Membranes in Low CO_2 Concentration Gas Mixtures Under Humid Conditions. *J. Membr. Sci.* **2017**, *525*, 290−297.
(23) Recker, E. A.; Green, M.; Soltani, M.; Paull, D. H.; McManus, G. J.; Davis, J. H.; Mirjafari, A. Direct Air Capture of CO_2 via Ionic Liquids Derived from "Waste" Amino Acids. *ACS Sustainable Chem. Eng.* **2022**, *10*, 11885−11890.
(24) Kosmulski, M.; Gustafsson, J.; Rosenholm, J. B. Thermal Stability of Low Temperature Ionic Liquids Revisited. *Thermochim. Acta* **2004**, *412*, 47−53.
(25) Kamavaram, V.; Reddy, R. G. Thermal Stabilities of Di-Alkylimidazolium Chloride Ionic Liquids. *Int. J. Therm. Sci.* **2008**, *47*, 773−777.
(26) Cao, Y.; Mu, T. Comprehensive Investigation on the Thermal Stability of 66 Ionic Liquids by Thermogravimetric Analysis. *Ind. Eng. Chem. Res.* **2014**, *53*, 8651−8664.
(27) Parajó, J. J.; Teijeira, T.; Fernández, J.; Salgado, J.; Villanueva, M. Thermal Stability of Some Imidazolium $[NTf_2]$ Ionic Liquids: Isothermal and Dynamic Kinetic Study Through Thermogravimetric Procedures. *J. Chem. Thermodyn.* **2017**, *112*, 105−113.
(28) Bhattacharyya, S.; Shah, F. U. Thermal Stability of Choline Based Amino Acid Ionic Liquids. *J. Mol. Liq.* **2018**, *266*, 597−602.
(29) Xu, C.; Cheng, Z. Thermal Stability of Ionic Liquids: Current Status and Prospects for Future Development. *Processes* **2021**, *9*, 337.
(30) Huang, Y.; Chen, Z.; Crosthwaite, J. M.; N.V.K. Aki, S.; Brennecke, J. F. Thermal Stability of Ionic Liquids in Nitrogen and Air environments. *J. Chem. Thermodyn.* **2021**, *161*, 106560.
(31) Keßler, M. T.; Gedig, C.; Sahler, S.; Wand, P.; Robke, S.; Prechtl, M. H. G. Recyclable Nanoscale Copper(I) Catalysts in Ionic Liquid Media for Selective Decarbozylative C−C Bond Cleavage. *Catal. Sci. Technol.* **2013**, *3*, 992−1001.
(32) Taha, M.; Quental, M. V.; e Silva, F. A.; Capela, E. V.; Freire, M. G.; Ventura, S. P. M.; Coutinho, J. A. P. Good's buffer ionic liquids as relevant phase-forming components of self-buffered aqueous biphasic systems. *J. Chem. Technol. Biotechnol.* **2017**, *92*, 2287−2299.
(33) Kohno, Y.; Kanakubo, M.; Iwaya, M.; Yamato, Y.; Makino, T. Ionic Liquid Mixtures for Direct Air Capture: High CO_2 Permeation Driven by Superior CO_2 Absorption with Lower Absolute Enthalpy. *ACS Omega* **2022**, *7*, 42155−42162.
(34) Xie, W.; Xie, R.; Pan, W.-P.; Hunter, D.; Koene, B.; Tan, L.-S.; Vaia, R. Thermal Stability of Quaternary Phosphonium Modified Montmorillonites. *Chem. Mater.* **2002**, *14*, 4837−4845.
(35) McDonald, J. L.; Sykora, R. E.; Hixon, P.; Mirjafari, A.; Davis, J. H. Impact of Water on CO_2 Capture by Amino Acid Ionic Liquids. *Environ. Chem. Lett.* **2014**, *12*, 201−208.
(36) Bragg, P. D.; Hough, L. The Oxidation of Proline, Hydroxyproline, and N-Methylglycine with Periodate. *J. Chem. Soc.* **1958**, 4050−4053.
(37) Zhang, X.; Chingin, K.; Zhong, D.; Liang, J.; Ouyang, Y.; Chen, H. On the Chemistry of 1-Pyrroline in Solution and in the Gas Phase. *Sci. Rep.* **2017**, *7*, 7675.
(38) Zhang, X.; Ji, Y.; Zhang, Y.; Liu, F.; Chen, H.; Liu, J.; Handberg, E. S.; Chagovets, V. V.; Chingin, K. Molecular Analysis of Semen-Like Odor Emitted by Chestnut Flowers Using Neutral Desorption Extractive Atmospheric Pressure Chemical Ionization Mass Spectrometry. *Anal. Bioanal. Chem.* **2019**, *411*, 4103−4112.
(39) Dai, Z.; Noble, R. D.; Gin, D. L.; Zhang, X.; Deng, L. Combination of Ionic Liquids with Membrane Technology: A New Approach for CO_2 Separation. *J. Membr. Sci.* **2016**, *497*, 1−20.

https://doi.org/10.1021/acsomega.3c02116
ACS Omega 2023, 8, 21154−21161